ORIGINAL ARTICLE

CrossMark

Sedimentary proxies for Pacific water inflow through the Herald Canyon, western Arctic Ocean

Henrik Swärd[1,2] · Matt O'Regan[1,2] · Christof Pearce[3] · Igor Semiletov[4,5] · Christian Stranne[1,2] · Henrik Tarras[1] · Martin Jakobsson[1,2]

Abstract
Pacific water inflow to the Arctic Ocean occurs through the shallow Bering Strait. With a present sill depth of only 53 m, this gateway has been frequently closed during glacial sea-level low stands of the Pleistocene. Here, we investigate the sedimentological and mineralogical response to sea-level rise and the opening of the Bering Strait during the last deglaciation in a 6.1 m-long marine sediment core (SWERUS-L2-4-PC1) from the Herald Canyon. Grain size data indicate an abrupt erosional contact at 412 cm down core that likely formed when Pacific waters first started to flow into the Arctic Ocean around 11 cal ka BP, and was topographically steered into the Herald Canyon. A transitional unit between 412 and 390 cm appears to be a condensed interval with minimal local sedimentation. The underlying sediments, deposited in a shallow, river-proximal setting, exhibit a rather uniform bulk and clay mineral composition similar to mineral assemblages from surface sediment samples of the Chukchi Sea. Enhanced contributions from Pacific waters above 390 cm (< 8.5 cal ka BP) are reflected by elevated chlorite/illite and (chlorite + kaolinite)/illite ratios, and are anti-correlated with intervals of higher illite/smectite ratios, interpreted as periods of enhanced advection of shelf transformed waters originating from the East Siberian Sea. Clay mineral changes in the Holocene drift sediments are best explained by the interplay between two origins for bottom waters in the Herald Canyon and are consistent with modern oceanographic observations.

Keywords Bering Strait · Flooding · Clay mineral assemblage · Herald Canyon · Chukchi Sea · Grain size

✉ Henrik Swärd
  henrik.sward@geo.su.se

1 Department of Geological Sciences, Stockholm University, Stockholm, Sweden

2 Bolin Centre for Climate Research, Stockholm University, 10691 Stockholm, Sweden

3 Department of Geosciences, Aarhus University, Aarhus, Denmark

4 Pacific Oceanological Institute, Far Eastern Branch of the Russian Academy of Sciences, Vladivostok 690041, Russia

5 Tomsk National Research Polytechnic University, Tomsk 634050, Russia

Introduction

The shallow Bering Strait (BS) is the only gateway for Pacific waters entering the Arctic Ocean, and one of two major gateways for oceanographic exchange between the Arctic and the World Oceans [37]. Different mean sea levels between the Pacific and the Arctic oceans [40], in combination with wind-driven processes [1, 12], drive a 1.1 Sv net influx of Pacific water through this gateway [47]. The relatively fresh, warm and nutrient-rich Pacific water influences ocean stratification [3], sea-ice melting [46] and biological productivity [43] in the western Arctic Ocean.

The estimated 120 m global sea-level rise [15, 24] following the last deglaciation flooded many low-lying landmasses in both hemispheres and opened new waterways. The shallow sill depth of the BS (− 53 mbsl) implies that it was exposed during the last glacial period and in many of the preceding glaciations of the Pleistocene. The landmass exposed between Alaska and Chukotka during glacial sea-level lowstands was referred to as Beringia by Hultén

[20]. This area has since commonly been called the Beringia Land Bridge, while the term Beringa alone is used for the entire shallow area comprising the present shelves of the Bering Sea, the Chukchi Sea (CS), the Beaufort Sea and the East Siberian Sea (Figs. 1, 2a). Increasing sea levels and the resulting flooding of the Beringia Land Bridge and opening of the Pacific–Arctic connection through the BS are thought to have affected human/animal migration routes [17] and climate stability [12]. Although previously assigned to a Younger Dryas (YD) age (12.9–11.7 cal ka BP) [14, 22], new geological data reveal that the opening of the BS seaway occurred later, around 11 cal ka BP [21]. This younger date agrees with paleo sea-level models, using the present topography/bathymetry with no isostatic adjustment in the region (Fig. 2b) [26] and implies that most previous studies addressing the consequences for BS inflow focused on an older time interval. Identifying sedimentologic and mineralogic proxies for periods of enhanced Pacific water inflow is an important step toward identifying the presence and/or intensity of Pacific water inflow in the geologic past using marine sediment cores.

One approach to this is the use of clay mineral assemblages as a provenance tool to identify Pacific-sourced waters (e.g., [23, 29–32, 41, 48]). Higher levels of chlorite and smectite are found in surface sediments from the CS (Fig. 3a) compared to adjacent areas to the east, west and north. These are explained by transport of fine-grained sediments from high-chlorite and high-smectite bearing regions in the Bering Sea [30–32, 39]. River runoff from the Chukchi Peninsula through erosion of volcanic rocks in the Okhotsk–Chukotka volcanic belt is suggested as the leading cause for the high smectite contents [41]. Sediments from the CS also exhibit lower illite contents compared to the sediments of the East Siberian Sea (ESS) (Fig. 3a) [41, 42]. The abundance of illite in ESS sediments has been attributed to riverine input from the Indigirka and Kolyma rivers (71 and 59% illite respectively) [30, 38] draining illite-rich lowlands [42] (Fig. 1). Due to these recognized clay mineral abundance variations, the opening of the BS has been suggested to result in a notable increase in the chlorite content of sediments that lie in the pathway of inflowing Pacific waters [23, 34, 48].

Today, the two major BS currents (Alaskan and Anadyr currents) split into four branches as they cross into the Arctic Ocean (Fig. 1) [10, 44, 45]. The strong Alaskan Coastal Current continues along the coast of Alaska with one branch passing into the Central Channel between Herald and Hanna Shoal (Fig. 1). The weaker Anadyr Current continues toward the Herald Canyon but also branches into the Long Strait south of Wrangel Island (Fig. 1). Sea-level reconstructions suggest that the Herald Canyon should have been a major pathway for the primordial waterway that formed during deglacial sea-level rise that ultimately led to the opening of the BS (Fig. 2a, b) [26, 35].

In 2014, the SWERUS-C3 expedition (SWERUS-C3: Swedish–Russian–US Arctic Ocean Investigation of Climate–Cryosphere–Carbon Interactions) on the Swedish icebreaker *Oden* recovered sediment core SWERUS-C3-L2-4-PC1 (Henceforth: 4-PC1) from 120 mbsl in the Herald Canyon (Fig. 1) [9, 21]. The core was taken from a drift deposit on the eastern flank of the Herald Canyon [21]. This core contained a major sedimentological and faunal transition between 412 and 400 cm depth [9, 21] that was linked to the high-resolution acoustic stratigraphy of the site and interpreted as marking the opening of the BS [21]. Radiocarbon dating of this transition provided a new age for the final opening of the BS [21]. The main evidence for a BS response in 4-PC1 was the sudden increase in biogenic silica (BSi), indicating the onset of high-nutrient Pacific water inflow and simultaneous decrease in $\delta^{13}C$ caused by the shift from a coastal to fully marine environment [21].

Here, we present new grain size, X-ray diffraction and biogenic silica data from 4-PC1. These data permit a detailed description of the core's sedimentological and depositional units and evaluation of the sediment and mineral compositional changes during the sea-level rise and flooding of the BS. Our study aims to identify/test sediment provenance and/or compositional changes that may have regional significance for reconstructing periods of Pacific water inflow in other marine sediment records.

Preliminary stratigraphy and chronology of 4-PC1

The 6.1 m piston core, 4-PC1, was recovered on the eastern slope of Herald Canyon, 160 km northeast of Wrangel Island (175°43.6′W 72°50.3′N) at a water depth of 120 m (Fig. 1). The general sediment and acoustic stratigraphy was presented by Jakobsson et al. [21], and a short summary is provided here. 4-PC1 is described by two major sedimentologic units (upper A and lower B), originally identified by changes in physical and geochemical properties occurring between 412 and 400 cm depth (Fig. 4a, b). Unit B was further divided into subunits B_1 and B_2 based on an increase in shear strength, magnetic susceptibility and bulk density between 513 and 503 cm core depth [21] (Fig. 4a).

Three major acoustic units are identified in the sub-bottom profile crossing the core site [21]. The acoustically chaotic lowermost unit is interpreted to have been formed contemporarily with the Last Glacial Maximum or late Glacial sea-level lowstand. A deglacial transgressive deposit constitutes the middle unit, which thickens toward the east, and is condensed at the coring site. This develops into the acoustically well-stratified upper unit reflecting a continuous
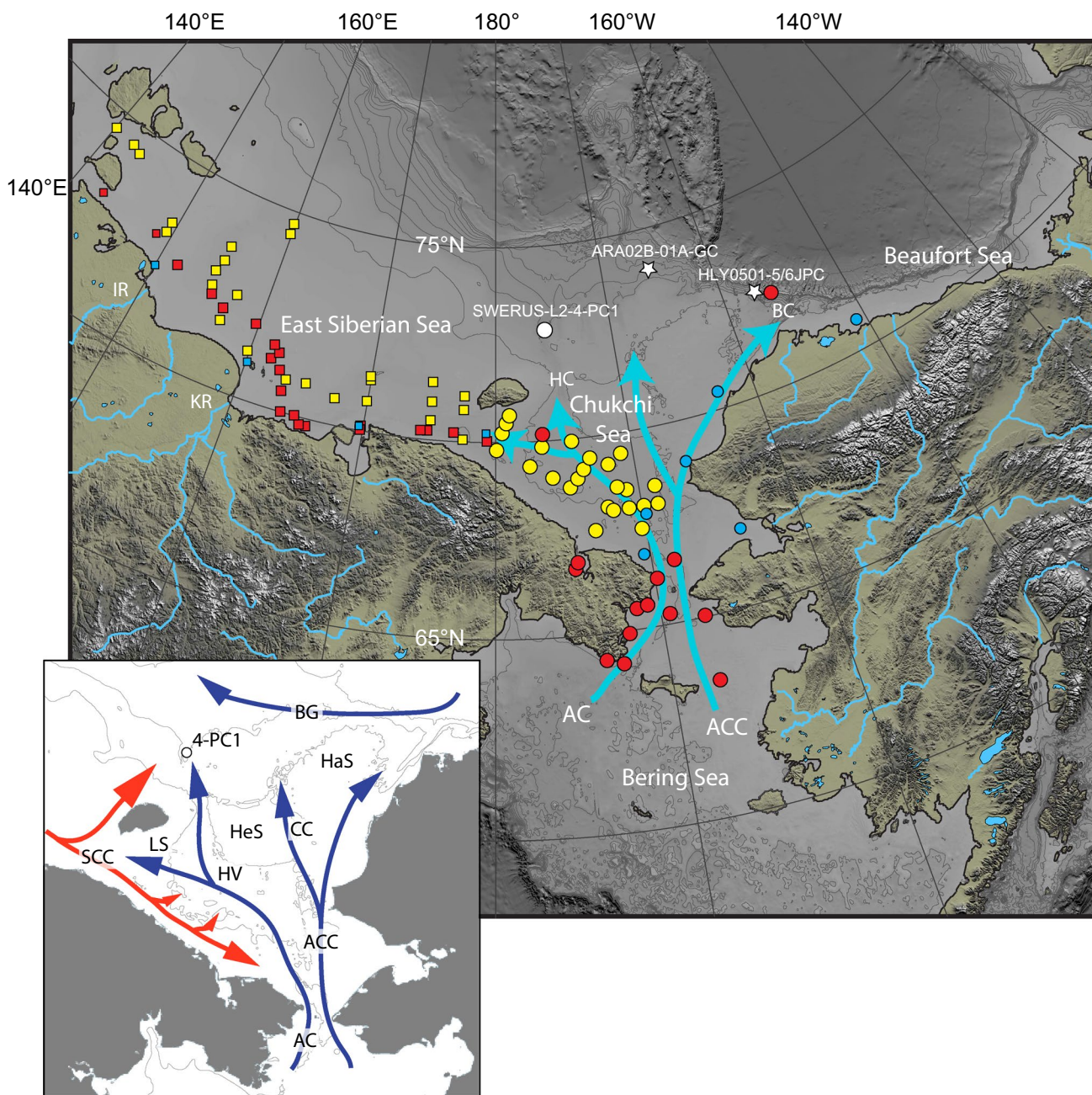
Fig. 1 Map of the study area. White circle indicates the location of SWERUS-L2-4-PC1. Rectangles indicate mineral samples from the East Siberian Sea, and circles indicate samples from the Chukchi and Bering Seas. Red samples (clay minerals) from Wahsner et al. [42], yellow samples (clay minerals) from Viscosi-Shirley et al. [41] and blue samples (bulk minerals) from Darby et al. [11]. Arrows show the major branches and pathways of Pacific waters. White stars indicate locations of sedimentary records discussed in the paper. Inset shows details of the modern oceanographic currents in the area (redrawn from [10]). *IR* Indigirka River, *KR* Kolyma River, *HC* Herald Canyon, *BC* Barrow Canyon, *AC* Anadyr Current, *ACC* Alaskan Coastal Current, *SCC* Siberian Coastal Current, *LS* Long Strait, *CC* Central Channel, *HV* Herald Valley, *BG* Beaufort Gyre, *HeS* Herald Shoal, *HaS* Hannah Shoal

drape of sediments [21]. Core-seismic integration suggests that the acoustic upper/middle unit transition is analogous with the lithologic Unit A/B transition [21] (Fig. 4).

Micropaleontological analyses by Cronin et al. [9] reveal an abundance of river-proximal benthic foraminifera in Unit B₁, with more typical marine and shallow shelf species of benthic ostracod and foraminifera in Unit A. As such, the high bulk density and magnetic susceptibility sediments of Unit B represent deposition in a nearshore environment with organic carbon isotopes also indicating a larger terrestrial
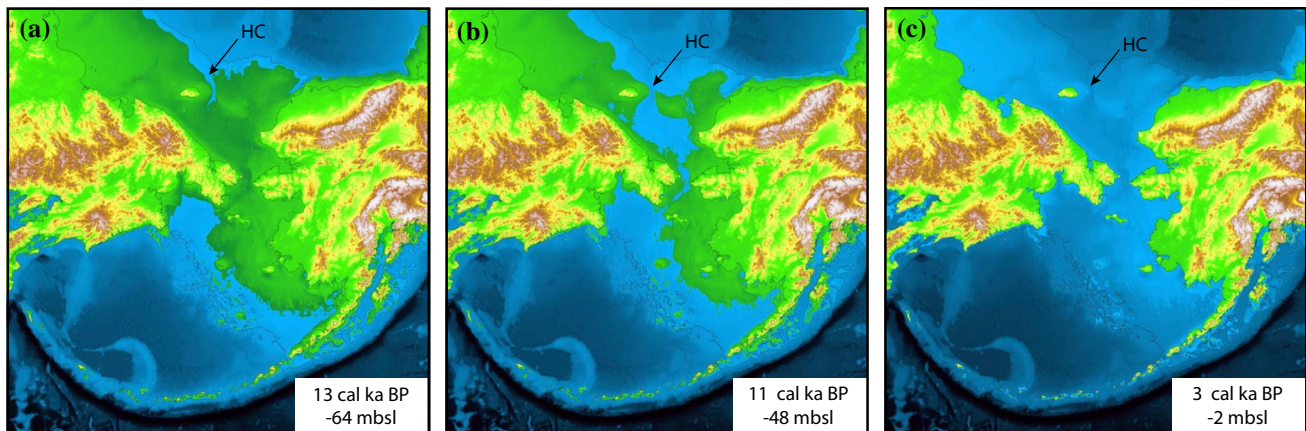
Fig. 2 Modeled time slices of deglacial sea-level rise and paleo-shorelines in the Arctic–Pacific region from Manley [26]. *HC* Herald Canyon. **a** 13 ka and −64 mbsl: Herald Canyon connected solely to the Western Arctic and surrounded by exposed landmass of Beringia. **b** 11 ka and −48 mbsl: at the opening of the Bering Strait, Herald Canyon was the only pathway for Bering Strait inflow into the Arctic Ocean. **c** 3 ka and −2 mbsl: full marine deep-sea environment in the Herald Canyon

input of organic matter (Fig. 4b). At the base of Unit A, BSi concentrations increase, and organic carbon isotopes transition toward a more marine signature. Together, these changes reflect sediment deposition in a more marine environment, where the inflow of nutrient-rich Pacific waters promoted increased productivity of surface-dwelling siliceous organisms [21]. The age model for 4-PC1 is based on nine AMS radiocarbon dated samples (mollusks and benthic foraminera) [9]. The bottom of the core is older than 12.1 cal ka BP based on a sample at 499 cm, i.e., 111 cm from the base of the core [9]. The flooding of the BS is dated at 11.1 cal ka BP, through upcore extrapolation to the middle of the transitional unit, at 407 cm core depth.

Methods

Grain size analysis

Grain size samples were taken at a resolution of 1 cm throughout 4-PC1. The bulk sediment samples were disaggregated in a combined pretreatment using sodium metaphosphate and ultrasonification. Grain size distribution was analyzed using a MasterSizer3000 laser diffractometer. The raw data was processed using GRADISTAT 8.0 [5] to obtain the geometric mean grain size and fractions of sand, silt and clay.

Biogenic silica (BSi)

To further constrain BSi across the Unit A/B transition [21], an additional 20 samples from 363.5 to 430.5 cm were analyzed. The samples were freeze dried before being treated with 1% Na_2CO_3 at 85 °C to dissolve the BSi based on the

methods of DeMaster [13] and Conley and Schelske [8]. Aliquots were taken after 3, 4 and 5 h of continuous dissolution and Si subsequently measured using a Thermo ICP 6500 DUO at the Stable Isotope Lab, Department of Geological Sciences, Stockholm University. While the BSi dissolves completely in the first 1–2 h, the dissolution of minerogenic silica continues at a slower rate. In a concentration–time plot, the intercept of the extrapolated curve through the 3, 4 and 5-h data points gives the actual BSi concentration in the original sample. Although the uncertainty may approach as much as ± 20%, the method is considered to provide trends in sedimentary BSi [7].

X-ray diffraction (XRD)

A total of 25 samples were collected from 4-PC1, with a slightly higher sampling resolution across the transitional sequence between Units A and B. The samples were freeze dried and sent to Weatherford Laboratories in Stavanger, Norway, for preparation, XRD analysis and post-processing. Approximately, 10 mg of dried material was crushed using a pestle and mortar and further divided into a bulk and clay mineral portion. The bulk mineral portion was milled and spray dried to obtain maximum random orientation [19] before being analysed on a Bruker AXS D4 Endeavor X-ray diffractometer from 5° 2θ to 70° 2θ at a step size of 0.02° per step. The minerals were identified using MDI Jade™ 9+ software and ICDD PDF 4+ 2015 database and subsequently quantified using reference intensity ratios generated by mineral standards.

After disaggregation, the clay mineral portion was centrifuged leaving the < 2 μm fraction in the supernatant. Subsequently, the clay fraction was oriented on a filter and glycolated before being analyzed on the Bruker AXS X-ray

diffractometer from 2° 2θ to 30° 2θ at a step size of 0.02°. Finally, the sample was heated to 375 °C for 1 h and rescanned using the same parameters to identify smectite [28]. Discrete clay minerals as well as mixed-layer clays were identified using the procedures first proposed by Biscaye [4] and later refined by Moore and Reynolds [28]. Quantification of clay minerals was performed using mineral intensity factors generated by clay mineral standards [28].

Results

Grain size

The most notable feature of the grain size data is the abrupt increase in the sand content and mean size of sediments that occurs at 412 cm, where the abundance of sand-sized material peaks at ~20%. The mean grain size below 412 cm core depth varies between 5 and 8 μm (average 6 μm) with peaks (~8 μm) at 450–455 and at 600–605 cm (Fig. 4c). At 412 cm, the mean grain size increases abruptly to 11 μm after which a fining upward sequence occurs until somewhere between 390 and 360 cm.

The sand fraction mirrors the mean grain size data in Unit B and across the Unit B/A transition (Fig. 4f). At 360 cm and upward, the similarity ceases and the sand fraction attains a low and stable signal (<3.5%). The silt fraction does not exhibit any large variations in Unit B (55–60%) until the very top where a decrease at 412 cm counterbalances the increase in sand at the same level (Fig. 4e). Between 412 and 400 cm, the silt fraction is more variable (47–57%) but increases significantly at 400 cm from where it continues increasing until it accounts for 65–70% of the sediment volume above 360 cm. Unit A is almost exclusively composed of cyclic, alternating clay and silt-rich layers. These are best seen in the clay/silt ratio and are mirrored by other traditional current-sensitive grain size proxies, including the mean size of the sortable silt (Fig. 5a).

Biogenic silica

The nine lowermost samples (403.5–430.5 cm) show small variation in the range of 0.8–1.7 wt% BSi (Fig. 4b). A slightly higher BSi (2.8%) is noted at 398.5 cm, followed by a rapid upward increase over 18 cm between 398.5 and 380.5 cm. BSi stabilizes at ~15% between 363.5 and 380.5 cm. The BSi data fits the previously reported values from 362.5 to 432.5 cm (Fig. 4). Despite the uncertainty associated with the method, the results present a convincing progression toward higher BSi levels between 400 and 380 cm and a very good agreement with the low-resolution data previously published from the same core [21].

Mineralogy

The mineralogical composition of 4-PC1 is reported in wt% of the bulk samples (Supplementary material 1). Major minerals in 4-PC1 are quartz, feldspars, illite, chlorite and smectite (Fig. 6). Notable changes in mineralogy between Unit A and Unit B exist in the mineral assemblages and are seen by non-overlapping 1σ standard deviations for average mineral concentrations in the two sedimentary units (Fig. 6). The average quartz content is 24% (21.3–30.2%) in Unit A and 26% (22.7–29.4%) in Unit B, while feldspars (K-feldspars and plagioclases) constitute 20% (18.2–21.9%) and 19% (16.3–20.4%), respectively (Table 1; Fig. 6). The clay minerals are dominated by illite averaging 31% (25.5–35.2%) for Unit A and 33% (30.9–34.4%) for Unit B. Chlorite exhibits an average of 12% (8.5–15.5%) in Unit A and 10% (8.1–12.6%) in Unit B, while the smectite content varies from 7% (4.6–8.6%) in Unit A to 9% (8.0–10.5%) in Unit B. The average kaolinite content is 3% in both units, while the ranges differ slightly (Unit A: 2.1–4.6% and Unit B: 1.9–4.2%). Notable changes in mineralogy are also revealed in the minor constituents dolomite, pyrite and halite (Fig. 6). Halite exhibits an average of 0.7% in Unit B compared to 2.9% in Unit A. Dolomite and pyrite are only present in trace amounts in Unit B, while increasing to an average of 1.2 and 1.1%, respectively, in Unit A. Dolomite starts becoming quantifiable at 328.5 cm, while pyrite and others start

Table 1 Average bulk mineral composition (wt%) for sediments north and south of Bering Strait

Location	Ref.	Illite	Chl.	Kaol.	Smec.	Quartz	Feld.	Q/F	Calcite	Dol.	Pyrite	Halite	Other
4PC-1 Unit A	This study	31	12	3	7	24	20	1.2	0.3	1.2	1.1	2.9	1.7
4PC-1 Unit B	This study	33	10	3	9	26	19	1.4	0.3			0.7	
ESS shelf	[11]	27	8	2	9	27	26	1.0	–	0.1	–	–	0.3
CS and BS shelves	[11]	29	9	1	6	29	23	1.3	0.1	0.9	–	–	1.6
Beaufort shelf	[11]	27	7	1	8	36	8	4.7	8.9	4.7	–	–	0.5

Q/F quartz/feldspar, *ESS* East Siberian Sea, *CS* Chukchi Sea, *BS* Bering Strait

Table 2 Average clay mineral composition for surface sediments in the Western Arctic and Bering Sea

Location	Ref.	Illite (wt%)	Chlorite (wt%)	Kao-linite (wt%)	Smec-tite[a] (wt%)	C+K	K/C	(C+K)/I
4PC-1 Unit A	This study	59	22	6	13	28	0.26	0.48
4PC-1 Unit B	This study	59	19	6	16	24	0.30	0.41
Beaufort Sea shelf	[42]	62	22	14	3	36	0.69	0.57
Beaufort Sea shelf	[11]	59	16	3	23	19	0.17	0.29
ESS shelf	[42]	69	20	8	4	28	0.40	0.41
ESS shelf	[41]	62	23	7	9	30	0.30	0.48
ESS shelf	[9]	58	19	4	19	23	0.21	0.38
CS shelf	[42]	57	25	9	9	34	0.36	0.60
CS shelf	[41]	51	23	7	20	30	0.30	0.59
CS shelf	[11]	62	19	3	15	23	0.16	0.35
Bering Sea I	[32]	48			12	40		0.83
Bering Sea II	[32]	38			24	38		1.00
Bering Sea III	[32]	44			29	27		0.61
Bering Sea IV	[32]	30			27	43		1.43

C chlorite, *K* kaolinite, *I* illite

[a]mixed layered-clays

increasing at 407.5 cm. A significant upward increase of halite first occurs at 394.5 cm.

For comparison with other regional clay mineralogy records, the clay mineral wt% was normalized assuming that the < 2 μm grain size fraction is composed purely of clay minerals (Table 2). Unit A exhibits an average clay composition of illite 59%, chlorite 22%, mixed-layered clay (illite/smectite) 13% and kaolinite 6%. The corresponding clay composition for Unit B is illite 59%, chlorite 19%, mixed-layered clay (illite/smectite) 16% and kaolinite 6%. Mixed-layered clay contains both pure smectite (expandable clays) and illite/smectite mixtures. Here, we use the term smectite to indicate the mixed-layered clay, which is a common reporting procedure for Arctic Ocean sediment mineralogy [16, 39].

Ratios of bulk and clay minerals are commonly used as proxies for sediment provenance. In the Western Arctic Ocean commonly applied ratios include (1) the quartz/feldspar ratio (*Q/F*), which tends to increase in surface sediments as one moves from the Siberian to the North American margin [23, 48] and (2) the chlorite/illite or (chlorite + kaolinite)/illite ratio, which are elevated in the Bering Sea and southern CS (Fig. 3), with decreasing values in surface sediments moving north through the CS [23, 48]. Here, we also present the illite/smectite ratio, as it shows pronounced longitudinal variability (Fig. 3) as one crosses the ESS and enters the BS/CS.

All of these ratios appear to change across the Unit A to B transition, with different mean values and non-overlapping standard deviations (Fig. 7). There is also clearly a larger degree of variability in the clay mineral assemblages in Unit A. To determine whether these apparent changes are significant, Student's *t* tests were applied (Table 3). Prior to the *t* test, an *F* test was performed to determine which type of *t* test should be used (unequal or equal variance). The datasets were assumed to be unpaired (independent) and to have normal distributions (two-tailed data). Given a 95% confidence interval ($p < 0.05$), $(C + K)/I$ differs significantly between Unit A and Unit B, while *C/I, I/S* and *Q/F* differ significantly at a 99% confidence interval ($p < 0.01$) (Table 3).

Discussion

Grain size changes during sea-level rise and BS flooding

The general trend of mean grain size data in 4-PC1 highlights the transition from a nearshore shallow environment (Unit B) characterized by pulses of coarse-grained sediment from local runoff and ice rafting into a fully marine environment (Unit A) with a silt-dominated deep-sea sediment drift signature (Fig. 4). Jakobsson et al. [21] used the distinct change in δ^{13}C and BSi (Fig. 4b) to mark the opening of the BS and the inflow of biosilica-rich Pacific water between 412 and 402 cm. The actual date for this event was derived by extrapolating the age model from underlying radiocarbon dates to the midpoint (407 cm) of the transitional unit. Here, we have identified an abrupt

Fig. 3 Longitudinal plots of clay minerals and ratios from the ▶
East Siberian and Chukchi Seas. All data from Wahsner et al. [42]
and Viscosi-Shirley et al. [41]. **a** Clay mineral data. Green = illite,
blue = chlorite, red = smectite and purple = kaolinite. **b** Illite/smectite
ratios. **c** Chlorite/illite and (chlorite + kaolinite)/illite ratios

change in grain size at 412 cm, with a coarse base and fin-
ing upward sequence that strongly alludes to a period of
erosion or winnowing. This sedimentological horizon at
412 cm may represent an earlier age marker for the initial
opening of the BS. However, this is only 5 cm below the
level interpreted to represent the BS opening by Jakobsson
et al. [21]. Therefore, there is no significant age change
to the estimated flooding at 11.1 cal ka BP, as the main
source of error remains the unknown regional marine res-
ervoir age at that time.

Unit A is composed of drift sediments recognized in
the high-resolution acoustic stratigraphy of the site [21].
Consistent with this interpretation, the cyclic variations
seen in the clay and silt content of this unit (Fig. 4) appear
to be related to current-related sorting (Fig. 5). Periods
of enhanced bottom current speed are seen by a higher
mean size of the sortable silt ($\overline{SS}$) and a lower silt/clay
ratio [27]. Traditional grain size current proxies can be
difficult to interpret in the Arctic because of the imprint
and importance of sea ice-rafted sediments [18, 33]. Hass
[18] originally showed that the $\overline{SS}$ in deglacial and Holo-
cene sediments from the Yermak Plateau increased as
the ice-rafted sand component increased. Subsequently,
in studying a longer Pleistocene record from the Lomono-
sov Ridge, O'Regan et al. [33] illustrated a similar bias,
with the % sortable silt in the fine fraction, $\overline{SS}$, and the
coarse silt content, all being positively correlated with the
sand fraction, which is clearly of ice-rafted origin. This
later study showed that the same patterns were evident in
modern sea ice samples from the Arctic. In 4-PC1, sedi-
ments from Unit B show a similar correlation between
the sand content, $\overline{SS}$ and coarse silt components (Fig. 5b,
c), suggesting a substantial sea ice-rafting overprint.
However, in Unit A, the silt fraction components remain
uncorrelated to the sand fraction (Fig. 5b, c). This sup-
ports the interpretation that the observed cyclic grain size
variations are primarily driven by current-related sorting.

Mineralogy prior to Bering Sea flooding

When compared to the longitudinal variations in the clay
mineralogy of the ESS and CS shelves, the illite content
of 4-PC1 is similar to the CS end member (< 55%) but
does not exhibit the higher smectite levels (> 15%) of
this region (Figs. 3, 6). Kaolinite and chlorite contents
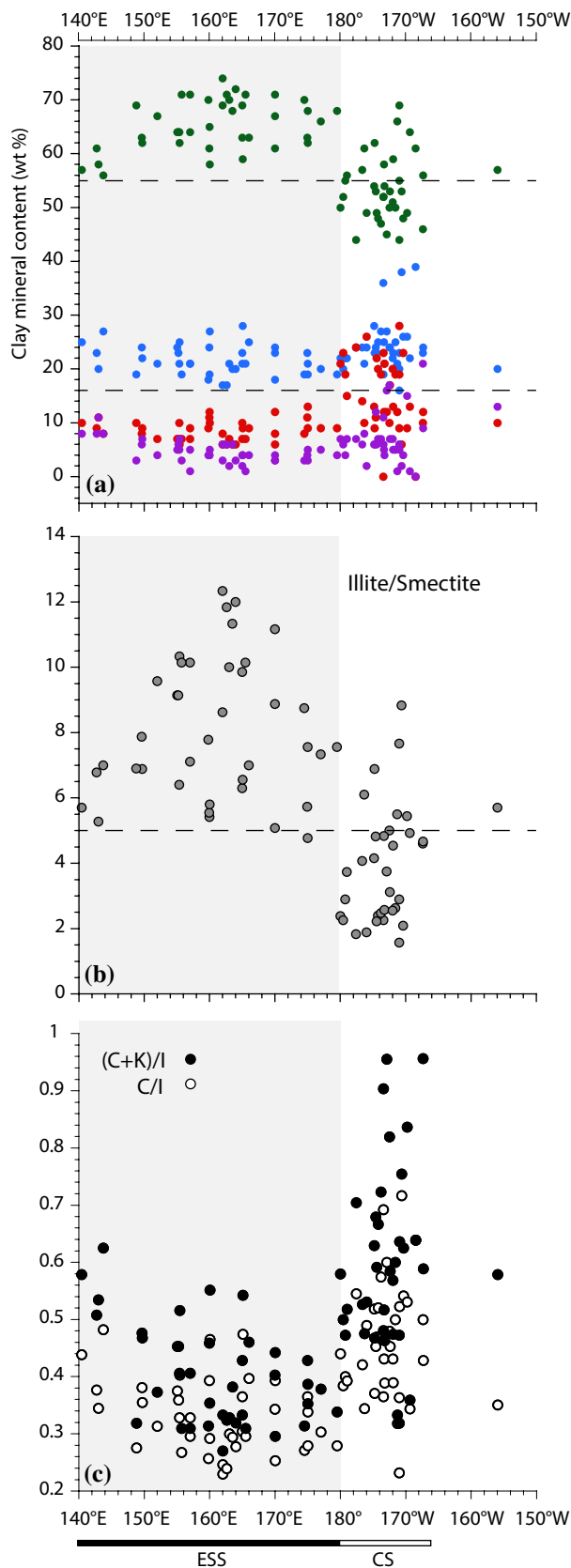of 4-PC1 do not exhibit deviations from the general ESS/

Table 3 Results from F and t tests on average mineral assemblage ratios between Units A and B of 4-PC1

	$(C+K)/I$	C/I	I/S	Q/F
F test p value	0.04	0.04	0.002	0.42
F test result	Equal variance ($p > 0.005$)	Equal variance ($p > 0.005$)	Unequal variance ($p < 0.005$)	Equal variance ($p > 0.005$)
Type of t test	Two tailed, unpaired equal variance	Two tailed, unpaired equal variance	Two tailed, unpaired unequal variance	Two tailed, unpaired equal variance
t test p value	0.03	0.009	0.005	6×10^{-6}

CS trends, which tend to be indistinguishable from each other (Fig. 3). The illite/smectite ratio (I/S) can provide further information on the relationship among clay mineral assemblages along the Siberian coastline. Ratios > 5 characterize all ESS sediment samples, while a majority of the CS I/S ratios are < 5 (Fig. 3). Our data reveal an I/S ratio of < 5 for almost all samples. (Fig. 7). These comparisons indicate that the clay mineralogy of 4-PC1 shows a close resemblance to a general CS clay mineralogy with respect to illite, chlorite, kaolinite and I/S ratio.

Mineralogy and composition after Bering Sea flooding

The new BSi data show a gradual increase through the transitional unit, stabilizing between 10–15% around 370.5 cm (Fig. 8). This closely corresponds to other geochemical ($\delta^{13}C$) and mineral assemblage (I/S, Q/F) indicators (Fig. 8). It is difficult to interpret the exact timing of these changes, given the prolonged period of limited deposition inferred by the current radiocarbon constraints between 412 and 390 cm. However, if the radiocarbon date at 399 cm (2σ: 8105–9075 cal a BP) is accepted [9], the implication is that the major sedimentologic and mineralogic changes did not stabilize until a few thousand years after the initial flooding of the Bering Strait. Median calibrated ages of the three overlying radiocarbon dates reported by [9] provide an estimated linear sedimentation rate of ~ 1.04 m/kyr ($R^2 = 0.975$). However, additional dating is required to constrain the period of erosion/winnowing and investigate short-term variations in sedimentation rate during the Holocene.

The accessory minerals identified by XRD analysis also changed after the flooding of the Bering Strait. Increased halite in Unit A (Table 1; Fig. 6) likely arises from the higher porosity of these sediments, but may also suggest increased pore water salinity. Pyrites are usually formed diagenetically during periods with increased input of organic carbon [2] and, hence, the increase in biologic production in Unit A [9, 21], and possible enhanced terrigenous organic matter deposition from runoff, is a probable cause for the appearance of pyrites (Table 1; Fig. 6). Finally, dolomite
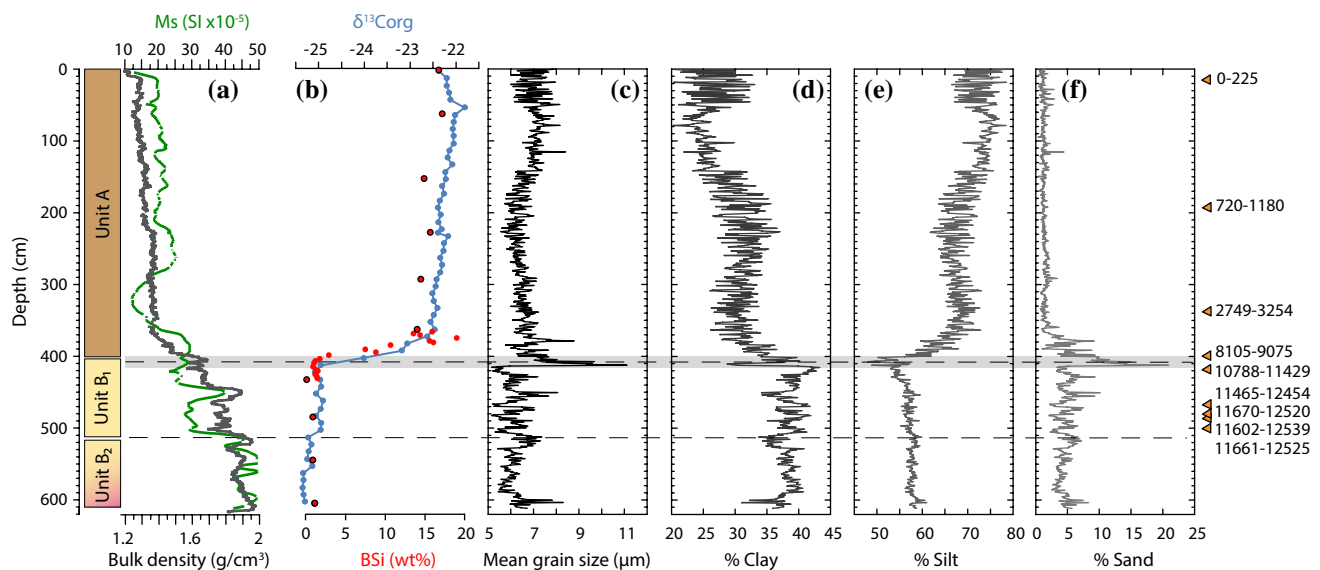

Fig. 4 Stratigraphic units, physical and chemical properties and grain size composition of 4-PC1. **a** Bulk density and magnetic susceptibility adapted from [21]. **b** Biogenic silica (BSi) and δ^{13}Corg. Red circles with black border and all δ^{13}Corg data are from [21]. Red circles without border are from this study. **c** Mean grain size calculated using geometric method of moments. **d** Clay fraction. **e** Silt fraction. **f** Sand fraction. Calibrated radiocarbon ages [9, 21] are presented using the calibrated 2σ error

Fig. 5 Current-related sorting in Unit A. **a** Silt/Clay and the mean size of the sortable silt (10–63 μm) with cyclic changes interpreted as a response to variations in bottom current strength. **b** Comparison of the coarse silt and sand content in sediments from Unit A (above 400 cm, brown circles) and Unit B (below 412 cm, yellow circles). **c** Comparison of the mean size of the sortable silt ($\overline{SS}$) and sand content in sediments from Unit A (above 400 cm, brown circles) and Unit B (below 412 cm, yellow circles). In both **b** and **c**, sediments from Unit B show a bias toward overall coarser silt fractions when the sand content increases. This is a recognized indicator of a substantial ice rafting overprint [18, 33]. Unit A sediments show no correlation between these parameters, suggesting a less substantial ice-rafting overprint
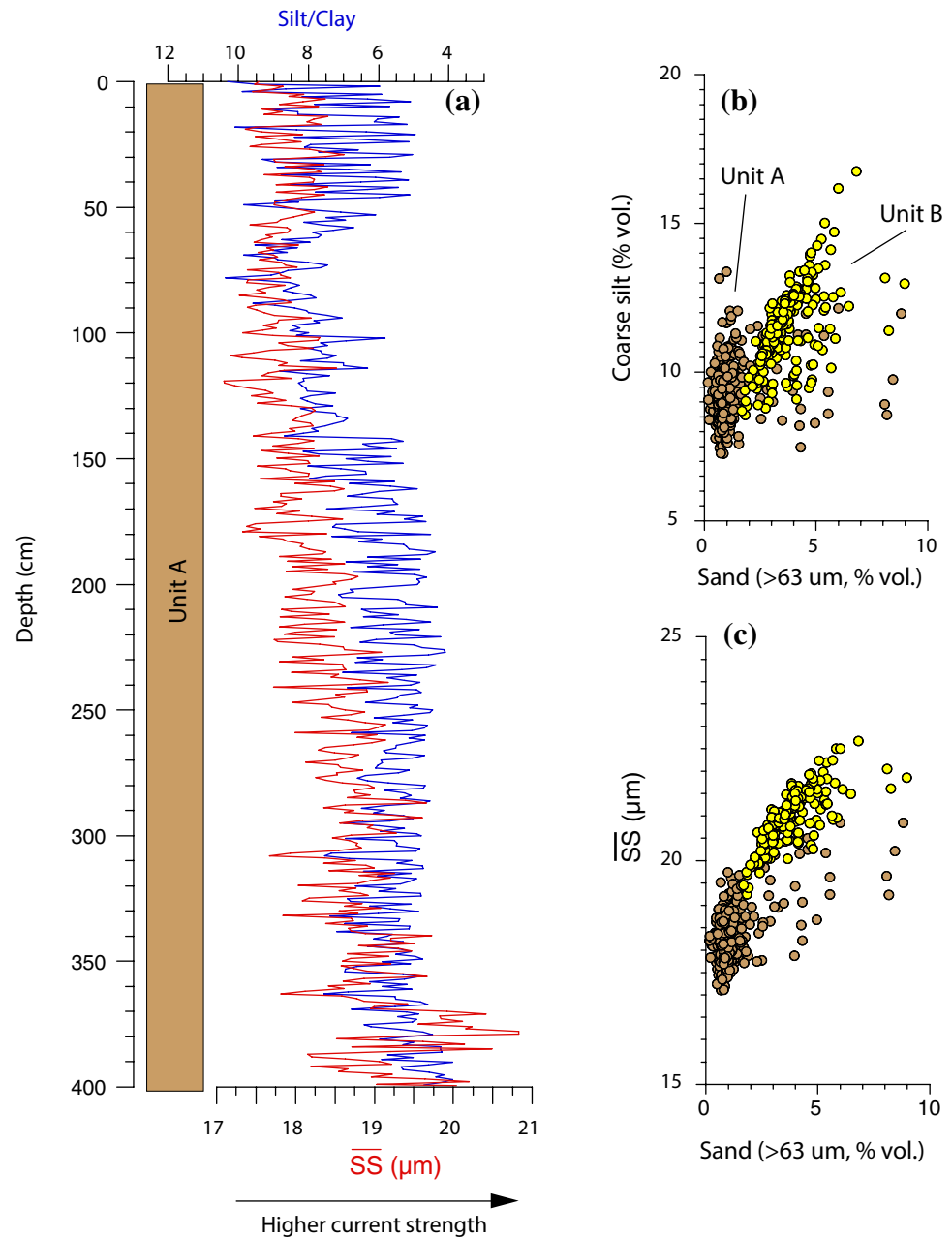
in Arctic sediments originates almost exclusively from the sedimentary bedrock of northern Canada and Greenland and is transported across the Arctic by sea ice via the clockwise Beaufort Gyre [39]. Hence, the appearance of dolomite in Unit A (Fig. 6) indicates a growing influence of the Beaufort Gyre in Herald Canyon area following the general sea-level rise. Darby et al. [11] also observe this influence in their CS and BS surface samples (Table 1).

The bulk mineralogy also illustrates a significant (99% confidence interval) decrease of quartz and increase in feldspars from Unit B to Unit A (Fig. 7; Table 3). The higher Q/F ratio in Unit B is consistent with the shorter distance from the core location in Herald Canyon to the paleo-shorelines

(Fig. 3). The importance of distance to the source for the Q/F ratio has been previously discussed [11] and is reflected in present-day nearshore data from the ESS and CS, which exhibits a similar level of quartz as the Unit B sediments (Table 1). An alternate possibility is that the lower Q/F ratio in Unit A arises from input of more feldspar-rich sediments originating from the ESS [11, 23]. This would be consistent with the higher average I/S that occurs in Unit A, suggesting a stronger ESS input.

The average C/I and $(C + K)/I$ ratios are also significantly higher in Unit A (Fig. 7), reflecting the contribution from Bering Strait inflow. However, they do not seem to change substantially until further upcore from 370.5 cm
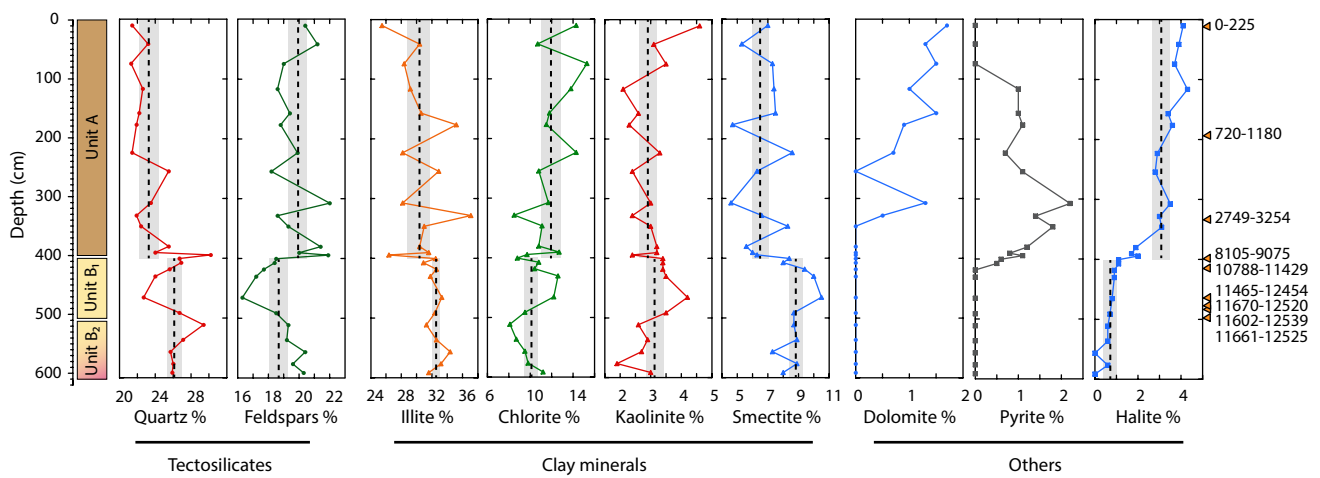
Fig. 6 Bulk mineralogy of 4-PC1 along with the lithostratigraphic units. Unit (A and B) averages and standard deviations are shown as dashed line/gray shaded area for each mineral. Calibrated radiocarbon ages [9, 21] are presented using the calibrated 2σ error
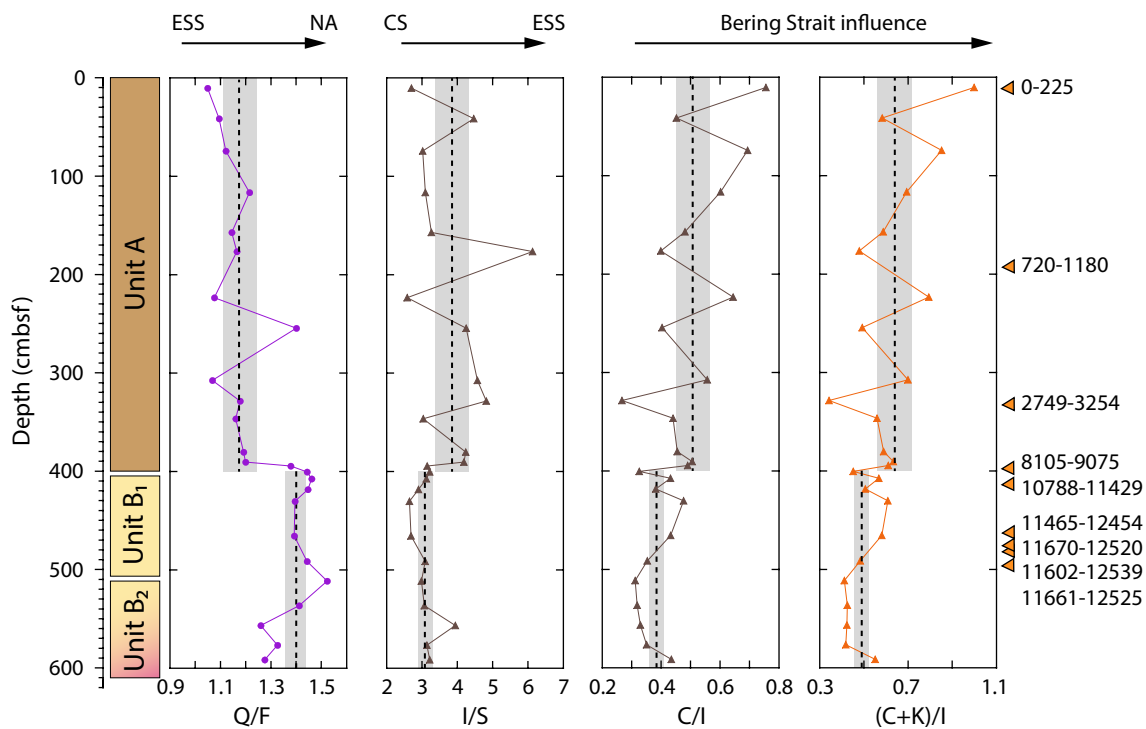

Fig. 7 Mineral ratios used to track changes in provenance of 4-PC1 sediments along with the lithostratigraphy and the calibrated radiocarbon ages. *Q/F* quartz/feldspar, *I/S* illite/smectite, *C/I* chlorite/illite, *(C + K)/I* (chlorite + kaolinite)/illite, *ESS* East Siberian Sea, *NA* North America, *CS* Chukchi Sea, *BSi* biogenic silica

and may suggest a moderate influence of BS inflow on sediment deposition in Herald Canyon until later in the Holocene (Figs. 7, 8). Temporal mineralogical records are rare and remain somewhat contradictory in this region of the Arctic. Increased chlorite levels between 9 and 6 ka in a sediment core from Barrow Canyon north of Alaska

(HLY0501-6JPC; Fig. 1) were attributed to increased inflow of Pacific waters as a response to insolation forcing [34]. Yamamoto et al. [48] investigated the same core, and while substantial variations in the chlorite/illite ratio exist throughout the Holocene, it remains difficult to see evidence for enhanced Pacific water inflow between 9 and
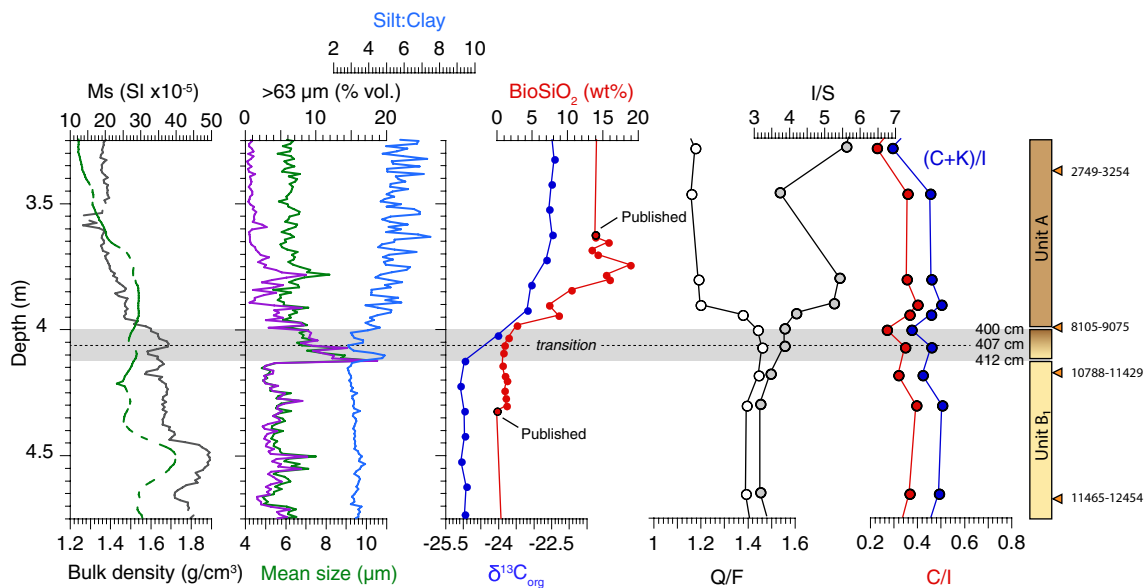
Fig. 8 Detailed view of the Unit B/A transition, including bulk density, magnetic susceptibility, mean grain size, sand fraction (>63 μm), δ13Corg, biogenic silica and mineral ratios. Lithostratigraphy and calibrated radiocarbon ages are shown on the left

6 ka. These differences may originate from differences in the applied age model, or analytical techniques. However, a central CS sediment core (ARA02B-01A-GC; Fig. 1) revealed increased levels of C/I ratios between 6.0 and 3.6 ka which were interpreted as reflecting a period of increased Bering Strait inflow [48]. The generally low sampling resolution in Holocene sediments from 4-PC1, and existing uncertainties in the age model, prevent a more detailed reconstruction of Pacific water inflow at this site.

Origin of mineralogic variability in Holocene sediments

At the resolution of this study, after the inundation of the CS and ESS and opening of the Bering Strait, clay mineral assemblages in 4-PC1 indicate both alternating periods of increased contributions from the BS and the ESS. Intervals of higher C/I and (C+K)/I (BS signature), are anti-correlated with intervals of higher I/S, which is an ESS signature (Fig. 7). This increased variability in the clay mineral assemblages, appears to capture pulses of BS and ESS sourced bottom waters (Figs. 6, 7). This is consistent with modern oceanographic observations, which have shown that bottom waters in Herald Canyon are not solely formed from the densification and sinking of Pacific waters, but from local sources in the CS and ESS [25, 36]. In particular, the northern deeper parts of the Herald Canyon (where 4-PC1 is located) is fed mainly by an easterly directed water current north of Wrangel Island (Fig. 1) [36]. This current is thought to derive from brine-driven convection caused by sea ice formation in the Wrangel Island polynya [6] and seems to

push the lighter Pacific water eastward over the Herald Shoal [36]. The variations in clay mineral assemblages in Unit A of 4-PC1 can therefore be explained by variable contributions from (1) the Bering Strait inflow with elevated C/I and (C+K)/I ratios and (2) shelf transformed waters from the East Siberian Sea bearing a higher I/S ratio. These shifts are likely related to variations in bottom water velocity interpreted from the cyclic, alternating clay and silt rich layers seen in the grain size data (Figs. 4, 5).

Conclusions

At the outset of this study, it was anticipated that deglacial sea-level rise and the opening of the Bearing Sea would result in a dramatic change in the mineralogy of sediments within Herald Canyon. Specifically, a large increase in the relative chlorite content was expected to occur after Pacific waters began to enter the CS. However, the results highlight a more complex view on the sources of Herald Canyon sediments. Certainly, there is a Pacific water signature captured in the sediments of Herald Canyon as is seen by the increase in the chlorite/illite and (chlorite + kaolinite)/illite ratios. However, these are interspersed with intervals of increased illite/smectite ratios, reflecting enhanced input from East Siberian sources. This is perhaps not overly surprising, as sea-level rise would not only allow inflow through the Bering Strait, but would also allow the establishment of the easterly-directed Siberian Coastal Current, which accounts for a significant portion of bottom waters found along the deeper, eastern flanks of

Herald Canyon today. The overall increased variability in the clay mineral assemblage after the BS opening highlights the combined inputs from these two source areas.

Compliance with ethical standards

Conflict of interest On behalf of all authors, the corresponding author states that there is no conflict of interest.

References

1. Aagaard K, Woodgate R, Weingartner T, Danielson S, Whitledge T, Johnson G (2006) Some controls on flow and salinity in Bering Strait. Geophys Res Lett 33:L19602. https://doi.org/10.1029/2006GL026612

2. Berner R (1984) Sedimentary pyrite formation: an update. Geochim Cosmochim Acta 48:605–615. https://doi.org/10.1016/0016-7037(84)90089-9

3. Beszczynska-Möller A, Woodgate RA, Lee C, Melling H, Karcher M (2011) A synthesis of exchanges through the main oceanic gateways to the Arctic Ocean. Oceanography 3:82–99

4. Biscaye PF (1965) Mineralogy and sedimentation of recent deep-sea clay in the Atlantic Ocean and adjacent seas and oceans. Geol Soc Am Bull 76:803–832

5. Blott SJ, Pye K (2001) GRADISTAT: a grain size distribution and statistics package for the analysis of unconsolidated sediments. Earth Surf Process Landf 26:1237–1248

6. Cavalieri DJ, Martin S (1994) The contribution of Alaskan, Siberian and Canadian coastal polynyas to the cold halocline of the Arctic Ocean. J Geophys Res 99:18343–18362

7. Conley DJ (1998) An interlaboratory comparison for the measurement of biogenic silica in sediments. Mar Chem 63:39–48. https://doi.org/10.1016/S0304-4203(98)00049-8

8. Conley DJ, Schelske CL (2002) Biogenic silica. In: Smol JP, Birks HJB, Last WM, Bradley RS, Alverson K (eds) Tracking environmental change using lake sediments. Developments in paleoenvironmental research, vol 3. Springer, Dordrecht, pp 281–293

9. Cronin TM, O'Regan M, Pearce C, Gemery L, Toomey M, Semiletov I, Jakobsson M (2017) Deglacial sea-level history of the East Siberian Sea Margin. Clim Past 13:1097–1110. https://doi.org/10.5194/cp-13-1097-2017

10. Danielson SL, Weingartner TJ, Hedstrom KS, Aagaard K, Woodgate R, Curchitser E, Stabeno PJ (2014) Coupled wind-forced controls of the Bering–Chukchi shelf circulation and the Bering Strait throughflow: Ekman transport, continental shelf waves, and variations of the Pacific–Arctic sea surface height gradient. Prog Oceanogr 125:40–61. https://doi.org/10.1016/j.pocean.2014.04.006

11. Darby DA, Myers WB, Jakobsson M, Rigor I (2011) Modern dirty sea ice characteristic and sources: the role of anchor ice. J Geophys Res 116:C09008. https://doi.org/10.1029/2010JC006675

12. De Boer AM, Nof D (2004) The Bering Strait's grip on the northern hemisphere climate. Deep Sea Res I 51:1347–1366. https://doi.org/10.1016/j.dsr.2004.05.003

13. DeMaster DJ (1991) Measuring biogenic silica in marine sediments and suspended matter. In: Hurd DC, Spencer DW (eds) Marine particles: analysis and characterization. American Geophysical Union, Washington, DC, pp 363–367

14. Elias SA, Short SK, Phillips RL (1992) Paleoecology of late-glacial peats from the Bering land bridge, Chukchi Sea shelf region, northwestern Alaska. Quat Res 38:371–378

15. Fairbanks RG (1989) A 17,000-year glacio-eustatic sea level record: influence of glacial melting rates on the Younger Dryas event and deep-ocean circulation. Nature 342:637–642. https://doi.org/10.1038/342637a0

16. Fagel N (2007) Clay minerals, deep circulation and climate. In: Hillaire-Marcel C, De Vernal A (eds) Proxies in late Cenozoic paleoceanography. Elsevier, Amsterdam

17. Goebel T, Waters MR, Rourke DH (2008) The late Pleistocene dispersal of modern humans in the Americas. Science 319:1497–1502. https://doi.org/10.1126/science.1153569

18. Hass HC (2002) A method to reduce the influence of ice-rafted debris on a grain size record from northern Fram Strait, Arctic Ocean. Polar Res 21(2):299–306

19. Hillier S (1999) Use of an airbrush to spray dry samples for X-ray powder diffraction. Clay Miner 34:127–135. https://doi.org/10.1180/000985599545984

20. Hultén E (1937) Outline of the history of arctic and boreal biota during the Quaternary Period: their evolution during and after the glacial period as indicated by the equiformal progressive areas of present plant species. Bokförlagsaktiebolaget Thule, Stockholm

21. Jakobsson M, Pearce C, Backman J, Barrientos N, Coxall H, De Boer A, Mörth CM, Rattray JE, Stranne C, O'Regan M, Cronin TM, Anderson LG, Björk G, Mayer LA, Nilsson J, Semiletov I (2017) Post-glacial flooding of the Bering Land Bridge dated to 11 cal ka BP based on new geophysical and sediment records. Clim Past 13:991–1005. https://doi.org/10.5194/cp-13-991-2017

22. Keigwin LD, Donnelly JP, Cook MS, Driscoll NW, Brigham-Grette J (2006) Rapid sea-level rise and Holocene climate in the Chukchi Sea. Geology 34:861–864

23. Kobayashi D, Yamamoto M, Irino T, Nam S, Park Y, Harada N, Nagashima K, Chikita K, Saitoh S (2016) Distribution of detrital minerals and sediment color in western Arctic Ocean and northern Bering Sea sediments: changes in the provenance of western Arctic Ocean sediments since the last glacial period. Polar Sci 10:519–531. https://doi.org/10.1016/j.polar.2016.07.005

24. Lambeck K, Rouby H, Purcell A, Sun Y, Sambridge M (2014) Sea level and global ice volumes from the Last Glacial Maximum to the Holocene. Proc Natl Acad Sci 111:15296–15303

25. Linders J, Pickart RS, Björk G, Moore GWK (2017) On the nature and origin of water masses in Herald Canyon, Chukchi Sea: synoptic surveys in summer 2004, 2008, and 2009. Prog Oceanogr 159:99–114. https://doi.org/10.1016/j.pocean.2017.09.005

26. Manley WF (2002) Postglacial flooding of the Bering Land Bridge: a geospatial animation: INSTAAR, University of Colorado, v1. http://instaar.colorado.edu/QGISL/bering_land_bridge. Accessed 11 Oct 2017

27. McCave IN, Hall IR (2006) Size sorting in marine muds: processes, pitfalls, and prospects for paleoflow-speed proxies. Geochem Geophys Geosyst 7(10):Q10N05. https://doi.org/10.1029/2006GC001284

28. Moore DM, Reynolds RC (1997) X-ray diffraction and the identification and analysis of clay minerals, 2nd edn. Oxford University Press, Oxford

29. Naidu A, Burrell D, Hood D (1971) Clay mineral composition and geologic significance of some Beaufort Sea sediments. J Sediment Petrol 41:691–694

30. Naidu A, Mowatt T, Creager J (1982) Clay mineral dispersal patterns in the north Bering and Chukchi Seas. Mar Geol 47:1–15. https://doi.org/10.1016/0025-3227(82)90016-0

31. Naidu A, Mowatt T (1983) Sources and dispersal patterns of clay minerals in surface sediments from the continental-shelf areas off Alaska. Geol Soc Am Bull 94:841–854

32. Naidu A, Wajda W, Han M, Mowatt T (1995) Clay minerals as indicators of sources of terrigenous sediments, their transportation and deposition: Bering Basin, Russian-Alaskan Arctic. Mar Geol 127:87–104. https://doi.org/10.1016/0025-3227(95)00053-2

33. O'Regan M, Sellén E, Jakobsson M (2014) Middle to late Quaternary grain size variations and sea-ice rafting on the Lomonosov Ridge. Polar Res 33:23672. https://doi.org/10.3402/polar.v33.23672

34. Ortiz JD, Polyak L, Grebmeier JM, Darby D, Eberl DD, Naidu S, Nof D (2009) Provenance of Holocene sediment on the Chukchi–Alaskan margin based on combined diffuse spectral reflectance and quantitative X-ray diffraction analysis. Glob Planet Change 68:73–84. https://doi.org/10.1016/j.gloplacha.2009.03.020

35. Peltier WR, Argus DF, Drummond R (2015) Space geodesy constrains ice age terminal deglaciation: the global ICE-6G_C (VM5a) model. J Geophys Res 120:JB011176. https://doi.org/10.1002/2014JB011176

36. Pickart RS, Pratt LJ, Torres DJ, Whitledge TE, Proshutinsky AY, Aagaard K, Agnew TA, Moore G, Dail HJ (2010) Evolution and dynamics of the flow through Herald Canyon in the western Chukchi Sea. Deep Sea Res II 57:5–26. https://doi.org/10.1016/j.dsr2.2009.08.002

37. Rudels B, Anderson L, Eriksson P, Fahrbach E, Jakobsson M, Jones EP, Melling H, Prinsenberg S, Schauer U, Yao T (2012) Observations in the Ocean. In: Lemke P (ed) Arctic climate change: the ACSYS decade and beyond, vol 43. Springer, Dordrecht, pp 117–198

38. Silverberg N (1972) Sedimentology of the surface sediments of the East Siberian and Laptev Seas. Dissertation, University of Washington

39. Stein R (2008) Arctic Ocean sediments: processes, proxies, and paleoenvironment. Elsevier, Amsterdam

40. Stigebrand A (1984) The North Pacific: a global-scale estuary. J Phys Oceanogr 14:464–470

41. Viscosi-Shirley C, Mammone K, Pisias N, Dymond J (2003) Clay mineralogy and multi-element chemistry of surface sediments on the Siberian-Arctic shelf: implications for sediment provenance and grain size sorting. Cont Shelf Res 23:1175–1200. https://doi.org/10.1016/S0278-4343(03)00091-8

42. Wahsner M, Müller C, Stein R, Levitan M, Shelekhova E, Ivanov G, Tarasov G (1999) Clay-mineral distribution in surface sediments of the Eurasian Arctic Ocean and continental margin as indicator for source areas and transport pathways—a synthesis. Boreas 28:215–233. https://doi.org/10.1111/j.1502-3885.1999.tb00216.x

43. Walsh JJ, McRoy CP, Blackburn TH, Coachman LK, Goering JJ, Henriksen K, Andersen P, Nihoul JJ, Parker PL, Springer AM et al (1989) The role of Bering Strait in the carbon/nitrogen fluxes of polar marine ecosystems. In: Rey L, Alexander V (eds) Proceedings of the sixth conference of the Comité Arctique International. E. J. Brill, Leiden, pp 90–120

44. Weingartner T, Aagaard K, Woodgate R, Danielson S, Sasaki Y, Cavalieri D (2005) Circulation on the north central Chukchi Sea shelf. Deep Sea Res Part II 52:3150–3174. https://doi.org/10.1016/j.dsr2.2005.10.015

45. Woodgate RA, Aagaard K, Weingartner TJ (2005) A year in the physical oceanography of the Chukchi Sea: moored measurements from autumn 1990–1991. Deep Sea Res II 52:3116–3149

46. Woodgate RA, Weingartner T, Lindsay R (2010) The 2007 Bering Strait oceanic heat flux and anomalous Arctic sea-ice retreat. Geophys Res Lett 37:L01602. https://doi.org/10.1029/2009GL041621

47. Woodgate RA, Stafford KM, Prahl FG (2015) A synthesis of year-round interdisciplinary mooring measurements in the Bering Strait (1990–2014) and the RUSALCA years (2004–2011). Oceanography 28:46–67. https://doi.org/10.5670/oceanog.2015.57

48. Yamamoto M, Nam SI, Polyak L, Kobayashi D, Suzuki K, Shimada K (2017) Holocene dynamics in the Bering Strait inflow to the Arctic and the Beaufort Gyre circulation based on sedimentary records from the Chukchi Sea. Clim Past 13:1111–1127. https://doi.org/10.5194/cp-13-1111-2017